

Breakup of an Axisymmetric Laminar Jet in the presence of non-ionic Surfactants.

Justin Walker and Richard V. Calabrese *

Department of Chemical and Biomolecular Engineering, University of Maryland, College Park, MD, 20742-2111 USA

Abstract:

The contacting of multiple liquid phases is a complex process, and one that is difficult to study experimentally. In this study, experiments are performed using the well studied axisymmetric jet system. Despite the extensive literature on the topic, the impact of surface active agents on jet breakup has received limited attention.

An extensive series of experiments with water-air and oil-water jet systems with surfactants has been performed. Jet length was found to increase with surfactant concentration, while droplet diameter was found to decrease (dependant on the jet regime). These results compare favourably with similar experiments involving high shear mixers.

Keywords: Multiphase mixing, Surfactants, Jet Breakup, Hydrodynamics

Introduction:

The contacting of multiple liquid phases is a complex process, and one that is difficult to study experimentally, requiring expensive specialized equipment, and difficult and lengthy cleaning and decontamination procedures due to the complex geometry of the mixing devices. It is therefore desirable to compliment experiments on mixers with a geometrically and hydrodynamically simpler analogue on which many experiments can be quickly and easily performed.

Many multiphase contactors (such as high shear mixers) function by forcing an immiscible fluid through an orifice or nozzle, or by otherwise destabilizing deformed droplets. Many of these processes can be mimicked on a fundamental level by the discharge of an immiscible axisymmetric laminar jet. Figure 1 shows RANS simulation results for a Silverson L4R Batch Rotor-stator mixer operating at 4000 RPM (reproduced from Yang and Calabrese (2009)). A strong exit jet is observed discharging from one of the stator slots. Figure 2 shows a similar RANS simulation from our study showing a liquid jet discharging from a circular capillary tube into a second immiscible phase. In either case, once exposed to the surrounding (matrix) phase, waves form on the surface of the jet causing it to destabilize.

* Corresponding author, rvc@umd.edu

In the case of the laminar jet, a certain distance from the capillary tip (hereafter referred to as the “breakup length”), the jet disintegrates into a series of discrete droplets. Often, the jet breaks up into large primary drops and smaller satellite droplets, resulting in a multi-modal droplet size distribution. Multi-modal distributions are not commonly observed in the high shear mixer environment due to the fact that droplets are re-entrained into the mixer (even in so-called 'single pass' mixing applications - see Murthy et al. (2009)).

The laminar axisymmetric jet was chosen as a model system partly due to its wide body of available literature. Jet breakup phenomena were first studied by Savart (1833) and Rayleigh (1879) in the 1800's. Many papers have been published over the years describing the theory of jet breakup, such as the paper by Tomotika (1935) or the volume by Chandrasekhar (1961). More recently, many studies have been performed using various computational simulations to better understand the mechanics of jet breakup, notable among these are Homma et al. (2006), and García and González (2008).

Despite the extensive literature on the topic of jet breakup, the impact of surface active agents on jet breakup has received limited attention, whether due to the system's inherent complexity or a poor understanding of the mechanics of the action of surface active agents themselves. A similar lack of literature on the subject of surfactants and mixing is what motivated this study in the first place. Thus, it is the goal of this study not only to develop a meaningful understanding of the effects of surfactants on the breakup of liquid droplets and threads, but to use that understanding to explain some of the previously unanswerable questions in the field of liquid-liquid dispersions.

Theory:

A cylindrical jet of fluid is hydrodynamically unstable, having a larger surface area than a sphere of equal volume. As such, surface tension drives the jet to break up. The dynamics of the system drive the jet to break up into a series of spheres, rather than a single one. According to Rayleigh, if the column becomes varicose with wavelength λ exceeding the circumference $2\pi r$ of the cylinder, the cylinder will decay into droplets such that each fluid ‘node’ comprises one drop. Figure 3 shows the relevant geometry.

If the breakup of an inviscid fluid cylinder is assumed to be driven only by capillarity (e.g., the influence of the outer fluid is ignored), and we work in the jet's reference frame (e.g., the jet velocity in the axial direction is zero), the Navier-Stokes equations may be linearized and rearranged to form Equation 1 (see Eggers and Villermaux (2008) for a detailed derivation)

$$\omega^2 = -\frac{\sigma}{\rho r_0^3} (kr_0) \left[1 - (kr_0)^2 \right] \frac{I_1(kr_0)}{I_0(kr_0)} \quad (1)$$

where ω is the growth rate of the instabilities, σ is the interfacial tension between the jet fluid and its surrounding fluid, r_0 is the initial jet radius, and k is the wavenumber of the

instability. The most unstable wavenumber is found by locating the value of k which maximizes ω .

No longer assuming the jet to be inviscid, a similar derivation results in Equation 2.

$$\omega^2 = -\frac{\sigma\eta}{\rho r_0^3} [1 - \eta^2] \frac{I_1(\eta)}{I_0(\eta)} - \frac{3\mu k^2}{\rho} \omega \quad (2)$$

Where $\eta=kr_0$ is substituted for convenience and μ is the fluid viscosity. Equation 2 can be recast in dimensionless form:

$$w^2 = \eta(1 - \eta^2) \frac{I_1(\eta)}{I_0(\eta)} - 3\eta^2 Ohw \quad (3)$$

Drop size is predicted by finding the value of η_{\max} by the above method, and then using Equation 4, which is derived from a simple geometric reduction.

$$D^* = \frac{d_{drop}}{d_{jet,i}} = \left(\frac{3\pi}{2\eta_{\max}} \right)^{1/3} \quad (4)$$

All of the above arguments assume that the jet breaks up linearly into mono-sized droplets. In practice, this is not the case. In most situations, jets break up into large primary droplets separated by one or more satellite drops. Generally these satellite drops are much smaller than the primary drops and contribute less than 3% of the total volume of the system, so the linear theory above can be safely used to predict the primary droplet diameter. In order to predict the size of satellite drops, the full Navier-stokes equations need to be solved for both the inner and outer fluid, a computationally extensive exercise beyond the scope of this study.

The other relevant quantity when discussing jet breakup is the breakup length. Using the instability growth rate found above, coupled with knowledge of the jet's geometry and velocity, an estimate of the time until the instability grows to exceed the jet diameter can be made. This quantity is known as the breakup time. From the breakup time, the breakup length can be calculated by also knowing the jet velocity. Das (1997), working off the earlier results of Rayleigh (1879), derived the following expression for jet breakup length L_b :

$$L_b = \frac{U_n}{\omega} \ln \left(\frac{r_0}{\delta_0} \right) \quad (5)$$

where U_n is the average jet velocity, and δ_0 is the amplitude of an infinitesimal disturbance on the surface of the jet. Since the value of δ_0 cannot be determined experimentally, Das (1997) and Scheele and Meister (1968) both found that using

$\ln(r_0/\delta_0) = 6$ successfully predicted breakup lengths for liquid-liquid systems. For this prediction, the value of ω from Equation 1 or Equation 2 is used, as appropriate. The dimensionless breakup length L_b^* is found by dividing by the initial jet diameter:

$$L_b^* = \frac{We^{1/2}}{2w} \ln\left(\frac{r_0}{\delta_0}\right) \quad (6)$$

Homma et al. (2006) performed a direct numerical simulation of a jet of one liquid into a second, immiscible liquid, similar to our current experimental study. Their results showed three distinct regimes. At low flow rate (or Re), dripping flow occurred, where droplets are produced one at a time at the capillary tip. Above a critical flow rate (indicated by the first dashed line), a stable jet begins to form, which increases in length with increasing jet velocity (as predicted by Equation 5). Jets in this regime exhibit axisymmetric wave patterns. However, another transition occurs where asymmetric waves begin to occur (labelled '3-Dimensional Flow' in Figure 4), which destabilize the jet and reduce its breakup length. The jet ultimately transitions into atomizing flow at very high jet velocity (well beyond the range used in this study).

In our study, theoretical predictions are only possible in clean-water systems. This is due to the fact that the Ohnesorge and Weber numbers cannot be defined for a system where the interfacial tension is a function of interfacial age and surfactant diffusivity. Current theory is unable to reconcile the dynamic effect of surfactants.

Surfactants:

Our system of interest is a surfactant laden system, where the fluid surfaces are partially or completely coated with amphiphilic chemicals which significantly effect interfacial phenomena.

Surfactants are commonly modeled as having an ionic, hydrophilic 'head', and an organic hydrophobic 'tail'. Thus, when exposed to an aqueous interface, the molecules have a tendency to orient themselves such that the hydrophobic group protrudes from the aqueous phase into the neighbouring fluid phase. Figure 5 shows a sketch of this phenomenon.

Surfactants will tend to self-organize if their concentration is sufficiently high. Above the Critical Micelle Concentration (CMC), surfactants will spontaneously form micelles, spherical structures where the molecules organize to minimize the contact of the hydrophobic end of the molecule with the surrounding aqueous phase. A similar phenomena, reverse micelles, occur in oil-soluble surfactants where the hydrophilic (and thus lipophobic) head groups are within the micelle. Figure 6 shows sketches of normal and reverse micelles. Micelles are in equilibrium with free surfactant molecules in solution, so if the bulk concentration of surfactant changes – for example by the creation or destruction of new surfaces, or by the addition of chemical, micelles can break or form

to maintain the bulk free surfactant concentration at the critical micelle concentration. In this manner, micelles act as a surfactant buffer and maintain the bulk interfacial tension constant and any surfactant concentration above the CMC.

The primary action of surfactants is to act as a ‘bridge’ between phases, reducing the interfacial tension. Surfactant molecules also add rigidity to interfaces, as any change in surface area or orientation causes gradients in the surface concentration of surfactant, resulting in Marangoni stresses which oppose these changes. Depending on the diffusivity (from the bulk to the interface) of the surfactant in question, these Marangoni stresses can have significant effects on jet breakup, as they act to damp out surface oscillations and stabilize the jet against breakup.

Surfactants also have significant effects on drop coalescence (see Stone and Leal (1990), and Yang et al. (2001)). While this study is not specifically investigating droplet coalescence, there are frequently droplet collisions very close to the breakup of the jet that sometimes result in coalescence – especially the collision of energetic satellite drops with the larger, slower moving primary drops. Thus, when the droplet size is measured downstream from the breakup event, the droplets observed may be the product of coalescence events. Generally, the coalescence of a satellite drop with a primary drop does not significantly change the drop diameter of the primary drop due to the disparity in volume between them, so coalescence phenomena will only be discussed qualitatively.

The Critical Micelle concentration of a surfactant solution can be calculated by measuring the equilibrium surface tension of a surfactant solution with another phase, and fitting the plot of concentration vs. interfacial tension to the Langmuir - von Szyszkowski equation (equation 7 - Fainerman et al. (1998)) .

$$\sigma_{eq} = \sigma_0 - \Gamma_{\infty} RT \cdot \ln \left(1 + \frac{C}{a_L} \right) \quad (7)$$

where a_L is the Langmuir Constant. Figure 7, reproduced from Padron (2004), shows the fitting of Equation 7 to the concentration- σ curves for 3 different non-ionic surfactants. The CMC is taken to be the intersection point of the linear decay line and the constant IFT line. This method was used in our study to convert absolute surfactant concentrations into 'CMC units', which allows for direct comparison of the effect of surfactants with differing CMCs.

Experimental Setup:

Jet Breakup Experiments:

Silicone oil (Dow Corning 200 Fluid) with a nominal viscosity of 10 cSt (9.8 cP) was injected into otherwise still deionized water or aqueous surfactant solutions. Three capillaries were used to form the jets in this study, having inner diameters of 0.42mm, 0.60mm, and 0.84mm, respectively. The capillaries were all 51mm long; enough to

assure fully developed laminar flow profiles at the capillary tip. A 1 litre fluid reservoir, maintained at constant pressure through the use of a regulated nitrogen gas cylinder, was used to initiate the flow. The flow rate of the jet phase was controlled using a needle valve and monitored using a rotameter. Flow rates were varied from 5-30 ml/min, corresponding to Reynolds numbers from 20-2000, depending on the capillary and fluid in use. The test cell was fitted with watertight windows and filled completely with deionized water (or aqueous surfactant solutions). The fluid reservoir was filled with deionized water in order to maintain the calibration of the rotameter, and the secondary reservoir at the bottom of the test cell was filled with silicone oil. In this manner, water flowed from the fluid reservoir, through the metering valve and flow meter into the secondary chamber, where it displaced oil and slowly filled the secondary chamber. The displaced oil was forced out of the needle, creating an oil jet in the upper water-filled primary chamber. An overflow keeps the cell chamber at constant pressure. The entire apparatus was placed on top of a pneumatic vibration isolation table to prevent any ambient vibrations from being transmitted to the jet surface.

Two distinct CCD cameras were used to image droplets. A low frame rate (30 images per second), high resolution camera was used to measure breakup length and to quantify droplet population statistics. A high frame rate (up to 20,000 images per second), moderate resolution camera was employed to observe detailed breakup phenomena. High quality Nikkor SLR ('F'-mount) lenses of various focal lengths were utilized with both cameras. For lighting, a diffuse fluorescent lamp with an 85,000 Hz driver was utilized to ensure even backlighting and eliminate the usual 60 Hz oscillations in lighting intensity common with AC lamps. An automated image processing algorithm was used to acquire droplet geometry and population statistics. See Figure 8 for a detailed schematic diagram of the experimental apparatus. An automated algorithm is employed to analyze the images and report the equivalent spherical diameter of the droplets. A similar automated algorithm is utilized to calculate the breakup length.

The non-ionic surfactant used in this study was octyl phenol ethoxylate (commonly known by the trade name Triton X-100). This surfactant is insoluble in silicone oils and was added to the aqueous phase, meaning surfactant must diffuse from within the surrounding matrix phase to the oil jet interface. See Figure 7 for the effect of this surfactant on equilibrium interfacial tension and determination of the critical micelle concentration.

Interfacial tension measurements:

Dynamic and Static surface/interfacial tension measurements were performed using the pendant drop technique. For this purpose a cuvette constructed from 2"x3" glass microscope slides was filled with the desired ambient fluid (or left empty for surface tension), and a syringe filled with the droplet phase fluid was fitted to a needle with either a straight or hooked end, to accommodate either positive or negative buoyancies. Again, the entire apparatus was placed atop a pneumatic vibration isolation table. For equilibrium measurements, droplets were formed manually, and then the system was left for several minutes to reach equilibrium. After the system had equilibrated, several

images were acquired on the hanging drop using a high resolution CCD camera. The drop was then ejected and a fresh drop formed. This process was repeated several times to ensure good results. Figure 9 shows a schematic diagram of this procedure.

Equilibrium interfacial tension values were calculated from the drop images using a customized computer algorithm, based upon the algorithm created by Padron (2004).

Results and Discussion:

Experimental Verification - Water in air jets

An initial set of experiments were performed with the well documented system of water jets into otherwise quiescent air. Figure 10 shows the dimensionless breakup length as a function of Reynolds number (see Equation 8). Once the jet transitions from the dripping phase (where droplets fall off the tip of the capillary one at a time) into the jetting phase, breakup length increases linearly with Re , as observed in the literature Eggers and Villermaux (2008). Similarly, dimensionless droplet diameters were found to decrease with Reynolds number (see Figure 11), but show incomplete correlation with Re . Goldin et al. (1969) stated that droplet diameter is always dependant on the orifice diameter, so the scatter of the data is not unexpected given that 3 different diameter capillaries are used to generate this data. Reynolds number is defined by Equation 8:

$$Re = \frac{\rho U_n d_{jet,i}}{\mu} = \frac{4\rho Q}{\pi d_{jet,i}\mu} \quad (8)$$

Following the verification experiments, an extensive parametric study of the water-in-air system in the presence of surfactants was performed (see Walker and Calabrese (2009)).

Oil in Water Jets

Once verification experiments were completed, oil jets breaking up into water were investigated. Experiments were performed using 10 cSt Silicone Oil as the jet phase, into a quiescent phase of deionized water or aqueous solutions of Triton X-100 surfactant. A total of 81 experiments were performed, encompassing 3 capillary diameters, 3 flow rates, and 9 surfactant concentrations. Figure 12 shows the effect of Reynolds number on the dimensionless breakup length for a 10 cSt Silicone oil jet into deionized water. The line shown in this and subsequent plots is a trend line. Already a strong distinction between the water jets in air is clearly observed. In this case, at low Re , the jet is in the dripping flow regime, meaning individual drops are produced one by one on the tip of the capillary. As such, the measured jet length will periodically grow from nearly zero to the major axis of the hanging large drop until it detaches. These droplets are generally many times the diameter of the capillary on which they form, which results in an average dimensionless breakup length on the order of 6-10. Once the Reynolds number exceeds

about 50 (although somewhat dependent on the capillary diameter), a stable jet forms. The length of this jet then decreases with increasing Reynolds number. This agrees with the results seen in the direct numerical simulation of a liquid-liquid jet published by Homma et al. (2006) (see Figure 4). Homma explained that at Reynolds numbers below the maximum jet length, the waves present on the jet surface are primarily axisymmetric, and the jet length will increase rapidly with increasing flow rate. At the maximum jet length, asymmetric waves start to appear on the surface of the jet, primarily in the form of periodic 'wake' type structures. These structures destabilize the jet and subsequently reduce its length with increasing Reynolds number. Figure 13 shows the effect of Reynolds number on the droplet size. Reynolds number is used on the abscissa in these plots because the more common Weber or Capillary numbers are undefined for a surfactant laden system, since the value of the interfacial tension is not constant. Since the Reynolds number incompletely correlates the experiments performed with different capillary diameters, subsequent results will be separated, and we will use the capillary diameter or flow rate, rather than the Reynolds number, to correlate the results.

Droplet sizes are represented by the dimensionless Sauter mean diameter, defined by equation 13.

$$D_{32}^* = \frac{1}{d_{jet,i}} \frac{\sum d_i^3}{\sum d_i^2} \quad (9)$$

The Sauter mean diameter strongly weights the mean toward the large droplets, which ignores the influence of satellite drops. This is desirable since experiments in the dripping flow regime will not produce satellite drops. Using the Sauter mean allows dripping flow and jetting flow experiments to be compared directly.

Figure 13 shows that while long jets were not found to occur until around $Re=50$, the droplet sizes resolve to the smaller size droplets at a lower Re - around 25. Further analysis of the high speed video imagery revealed that in this intermediate regime ($25 < Re < 50$), a very short, unstable jet formed that was of comparable length to the large hanging droplets found in the dripping flow regime. These short jets produced small droplets similar in size to those produced by the longer stable jets. In the stable jetting flow regime, droplet size was correlated to jet length, with longer jets producing larger droplets, and droplet size decreasing as jet length decreased at higher Reynolds numbers. This is contrary to the linear breakup theory presented above, which predicts that droplet size should be independent of jet velocity. However, it is obvious from our experimental observations that jet breakup is not driven exclusively by capillarity and that shear induced waves also play a role in determining the ultimate breakup frequency and breakup time. From the high speed video, it appears as though shear layer instabilities form very near the capillary tip. The effect of these shear layer instabilities is strongly dependant on the jet length. For longer length jets, these instabilities are damped out by viscous dissipation and the jet breakup is dominated by capillary (Rayleigh) instabilities. For very short jets, the breakup is dominated by shear layer instabilities. For jets of moderate length, the dominant instabilities are a product of the two waves.

In order to better understand the effect of shear layer instabilities, a CFD simulation was undertaken. Utilizing the commercial CFD package FLUENT and the Volume of Fluid (vof) method, a Reynolds Averaged Navier-Stokes (RANS) simulation was performed on a 67,000 node 2D mesh based on the geometry of the experimental cell. As in the experiment, the jet phase was an oil with the same viscosity, density, and surface tension as the 10 cSt Silicone Oil, and the continuous phase was water. Despite the short run time of the simulation, the formation of shear layer recirculation zones and asymmetric waves on the jet surface are clearly evident, as seen in Figure 14.

Figure 15 and Figure 16 shows the effect of surfactant concentration on the breakup length of a 10 cSt silicone oil jet into aqueous solutions of Triton X-100. The surfactant concentration of $1E-4$ represents the deionized water case. For clarity, the figures are broken up and organized by capillary diameter (Figure 15) and by relative flow rate (Figure 16). Note that for the flow rate groupings, the lowest, middle, and highest flow rates used for a given capillary are grouped together, meaning that the nominal flow rate in each figure is not the same for all 3 sets of data.

Figure 15A shows the effect of surfactant concentration on breakup length for the smallest capillary size - 0.41mm in diameter. This case represents the largest Re because of the small capillary diameter (when volumetric flow rate is held constant - see equation 8). As seen above, the intermediate flow rate produces the longest jet due to the presence of asymmetric waves on the higher velocity jet (see Figure 4).

In all cases, a pronounced increase in jet breakup length is noted with increasing surfactant concentration. Jet length is constant at concentrations below the CMC, and then increases strongly at concentrations above the CMC. The primary reason for this is that increasing surfactant concentration on the surface increases the magnitude of the Marangoni stresses, which act to oppose any change in the surface area. Thus, when a capillary wave attempts to cause the jet to break, the Marangoni stress resists the capillary forces and maintains the jet's diameter. As the capillary wave grows in magnitude further downstream it is able to overcome the Marangoni stress, but this results in a jet which is significantly longer than one which does not have sufficient surfactant coverage.

Since surfactant must diffuse from the surrounding aqueous phase to the jet surface, the effect of the bulk surfactant concentration strongly influences the jet breakup phenomena even at concentrations exceeding the CMC where the bulk interfacial tension will not change. The effect is synergistic in the sense that increasing surfactant concentration allows more surfactant to reach the jet's surface in the short breakup time (the increased concentration gradient results in a larger mass transfer flux from the bulk to the surface). This, in turn, stabilizes the jet, increasing the breakup time, which allows for yet more surfactant to diffuse to the surface, which further increases the breakup time, and so on. This is the reason for the very rapid increase in breakup length with increasing surfactant concentration. Clearly, at some point a plateau should be reached when the jet surface becomes saturated with surfactant so rapidly that further increases in surfactant concentration no longer have any beneficial effect on the jet breakup length. It appears as

though that plateau concentration has nearly been reached in certain conditions (for example Figure 15C), as the dimensionless breakup length did not increase as much between the 20 CMC and 50CMC values as for the 1CMC to 10 CMC and 10 CMC to 20 CMC ranges. At 50 CMC, the cloud point (maximum solubility limit) of the Triton X-100 surfactant has nearly been reached, so experiments at even higher surfactant concentrations are not possible.

One of the most interesting results is observed most clearly in Figure 16A. At low surfactant concentration, all three of these experimental conditions (the lowest flow rates tested for each capillary, respectively) fall within the dripping flow regime, as evidenced by the extremely short jet lengths. However, once the surfactant concentration exceeds the CMC, the jet is sufficiently stabilized to transition into the jetting regime, producing jets with dimensionless breakup lengths similar to conditions at much higher flow rates despite the fact that the Reynolds number is unchanged.

Another interesting result is that for the largest jet at it's highest flow rate (most easily observed in Figure 15C, the effect of surfactants is much less pronounced. Upon examining the high speed video of these experiments, there were strong shear layer instabilities and asymmetric waves present. Unlike the axisymmetric capillary waves, the asymmetric waves do not significantly change the interfacial area, and so are not as strongly opposed by the Marangoni stress. Once the asymmetric waves gain strength, they are able to induce strong recirculation zones in the outer fluid which tear large chunks of the jet off. These recirculation zones do not appear to be significantly opposed by the Marangoni stress and so, under these conditions, only a moderate increase in jet length with a significant amount of data scatter is observed. A similar, but less pronounced, effect is observable in Figure 15B when looking at the 0.60 mm capillary's highest flow rate. The image analysis in this case showed some asymmetry to the jet, but not as much as with the 0.84 mm capillary.

Figure 17 and Figure 18 show the effect of surfactant concentration on the dimensionless Sauter mean diameter of droplets produced by the breakup of a 10 cSt silicone oil jet into aqueous solutions of Triton X-100, grouped again by capillary diameter and by flow rate, respectively. Once again the 1E-4 concentration represents the deionized water case. For the larger capillary diameters, dripping flow was observed at the lowest flow rate (see Figure 17B and Figure 17C), resulting in very large droplets being produced. As surfactant concentrations increase, these jets transition into the jetting phase and produce much smaller droplets. For jetting phase breakup, droplet size was found to increase with surfactant concentration. The same stabilization mechanism that allows the jets to grow to such large lengths is responsible for these large droplets. Downstream of the breakup event, the troughs of the jet waves are suppressed due to the Marangoni stress. This causes the second fluid node to be pushed into the forming drop on the tip of the jet, doubling it's size, instead of that drop pinching off. Under certain conditions, several fluid nodes can be 'pumped' into the forming droplet in this manner until the droplet, assisted by it's own buoyancy, detaches from the jet. This is much more like the droplet formation in a dripping flow mode than standard jetting flow. As with the jet length,

concentrations above the CMC are required to effect significant change in droplet diameter.

For jets breaking up in the asymmetric regime, no significant change in droplet diameter is observed. Figure 16C clearly shows that for the largest diameter jet, a slight increase in droplet diameter is observed for the 20 ml/min flow rate, and no increase is observed for the 30 ml/min flow rate. It appears as though the fluid thread detachment mechanism observed in the asymmetric jetting regime is not sensitive to surfactant concentration. It is also notable that this regime produces significantly larger drops than the axisymmetric jetting regime. This is shown most clearly in Figure 17C, where the 0.84 mm capillary produces droplets 2-3 times the size of those produced in the 0.41 mm capillary.

Figure 20 (reproduced from Padron (2004)) shows the effect of surfactant concentration on the Sauter Mean Diameter of droplets produced in a Silverson L4R batch rotor-stator mixer rotating at a moderately low speed (3000 RPM). For the 10 cSt silicone oil, an initial decrease in droplet diameter is seen with surfactant concentration, up to the CMC (dashed line). Increasing surfactant concentration above the CMC resulted in a slight increase in droplet diameter. This parallels the results seen in our experiments, especially for moderate flow rates when no flow regime transitions are observed (Figure 17B for example, where the minimum droplet size is observed just below the CMC). The changes are more pronounced in our current experiment, which is likely due to the fact that in the high shear mixer there is strong convective transport of surfactant to the droplet, so the rate limiting step for resolving Marangoni stresses is the transport of surfactant through the drop's boundary layer, while in our case there is no convective surfactant transport and we must rely on diffusion through the bulk aqueous phase.

Figure 20 (reproduced from Padron (2004)) shows the effect of surfactant concentration on the Sauter Mean Diameter of droplets produced in the same rotor-stator mixer rotating at a high speed (7000 RPM). Again, the results achieved in the rotor stator mixer for the 10 cSt oil closely match the results shown in the laminar jet, in this case the results in the high Re jets observed in Figure 17C. At all surfactant concentrations, there is essentially no effect on the droplet diameter observed in the high shear mixer. In our Jet experiments, no significant effect was observed either with jets operating in the asymmetric jetting regime. This implies that in the high shear mixer, a different breakup mechanism is occurring at high rotor speed than at lower rotor speed, and this secondary breakup mechanism is relatively insensitive to surfactant concentration. In the case of the jet we can observe that for the asymmetric jetting case the bulk fluid motion is what drives breakup, while at lower jet velocities (the dripping and axisymmetric jetting regimes), it is the dispersed phase motion that is ultimately responsible for jet breakup.

Conclusions:

Three distinct flow regimes were observed over the range of conditions studied. Figure 21 shows sample images of these different phases. The dripping flow regime occurs at low flow rates ($Re < 50$) when surfactant concentration is low. Axisymmetric jetting was observed at moderate flow rates, or at low flow rates and high surfactant concentration.

Asymmetric jetting was observed at high flow rates and was relatively insensitive to surfactant concentration. The traditional prediction criteria for the transitions between these breakup modes (based on Weber number) cannot be used in this study due to the inability to define the Weber number for a system where the interfacial tension is a function of interfacial age.

The Axisymmetric Laminar jet has been shown to be a useful tool for analyzing surfactant laden liquid-liquid flows. Similar results have been observed in surfactant laden flows in rotor stator mixers as with liquid-liquid jets. At moderate flow rate or rotor speed, droplet size was found to decrease with increasing surfactant concentration, with droplet size increasing (or levelling off) at higher concentrations. At higher flow rates or rotor speeds, droplet size was not found to change with increasing surfactant concentration. In jets this was attributed to the fact that these high flow rate jets broke up due to asymmetric waves which are dominated by bulk phase movement.

Increasing surfactant concentration was found to increase Jet breakup length for all cases studied, however the largest increase was found at concentrations well above the critical micelle concentration. This was attributed to the short jet breakup time with respect to the time required for surfactant to diffuse to the oil-water interface from the bulk aqueous phase. High surfactant concentration synergistically increased jet breakup length by providing a much higher mass transfer flux, allowing more surfactant to diffuse to the surface, which elongated the jet and lengthened the jet breakup time, further allowing surfactant to diffuse.

Current theory regarding jet breakup is insufficient to predict droplet diameters or jet lengths in a system with surfactants, since the Weber number is a function of time. Development of a model to address this, utilizing either an empirical 'effective' viscosity or interfacial tension term, or some form of diffusive flux model, is essential for further study in this field. However, Lee et al. (2009) showed that for these sorts of non-steady surfactant diffusion situations, the kinetics of the surfactant's absorption onto the interface (generally considered to be instantaneous compared to diffusion) can be the rate limiting step under certain conditions. This further complicates any attempt to model this situation mechanistically, likely necessitating a semi-empirical model.

Other suggestions for future study include a series of experiments with increased viscosity ratios to compare with the work in the rotor-stator mixers, and a study with other surfactant types with a different diffusion rates to better characterize the effect of surfactant diffusion rate on jet breakup.

References:

- Chandrasekhar, S., "Hydrodynamic and hydromagnetic stability", Clarendon Press, Oxford,(1961), pp. 515-576.
- Das, T. K., "Prediction of jet breakup length in liquid-liquid systems using the Rayleigh-Tomotika analysis", *Atomization and Sprays* **7**(5) 549-559 (1997).
- Eggers, J. and E. Villermaux, "Physics of liquid jets", *Reports on Progress in Physics* (3) 1-79 (2008).
- Fainerman, V. B., E. H. Lucassen-Reynders, et al., "Adsorption of surfactants and proteins at fluid interfaces", *Colloids and Surfaces A: Physicochemical and Engineering Aspects* (143) 141-165 (1998).
- García, F. J. and H. González, "Normal-mode linear analysis and initial conditions of capillary jets", *Journal of Fluid Mechanics* **602**(-1) 81-117 (2008).
- Goldin, M., J. Yerushalmi, et al., "Breakup of a laminar capillary jet of a viscoelastic fluid", *Journal of Fluid Mechanics Digital Archive* **38**(04) 689-711 (1969).
- Homma, S., J. Koga, et al., "Breakup mode of an axisymmetric liquid jet injected into another immiscible liquid", *Chemical Engineering Science* **61**(12) 3986-3996 (2006).
- Lee, W., L. M. Walker, et al. "Adsorption Kinetics of Alkyl Polyethylene Oxide Surfactants at the Water-Oil Interface " in "Fundamentals of Interfacial Phenomena II - Surfactants and Liquid/Solid Interfaces", Nashville, TN, USA, 2009, AIChE Annual Meeting.
- Murthy, B. N., K. T. Kiger, et al. "Single Pass Drop Size Distributions Produced by a Multistage in-Line Rotor-Stator Mixer " in "Mixing in Multi-Phase Systems - Gas-Liquid and Liquid-Liquid Systems", Nashville TN, USA, 2009, AIChE Annual Meeting.
- Padron, G. A., "Effect of surfactants on drop size distributions in a batch, rotor-stator mixer". *Chemical and Biomolecular Engineering*, University of Maryland. College Park, Maryland. Ph.D. Dissertation,(2004)
- Rayleigh, L., "On the Capillary Phenomena of Jets", *Proceedings of the Royal Society of London* **29**(196-199) 71-97 (1879).
- Savart, F., "Mémoire sur la Constitution des Veins liquides lancées par des orifices circulaires en mince paroi (On the Formation of liquid jets issuing from circular orifices in thin plates)", *Annales des Chimie et des Physique* **53** 337-386 (1833).
- Scheele, G. F. and B. J. Meister, "Drop formation at low velocities in liquid-liquid systems: Part II. Prediction of jetting velocity", *AIChE Journal* **14**(1) 15-19 (1968).
- Stone, H. A. and L. G. Leal, "The effects of surfactants on drop deformation and breakup", *Journal of Fluid Mechanics Digital Archive* **220**(-1) 161-186 (1990).
- Tomotika, S., "On the Instability of a Cylindrical Thread of a Viscous Liquid Surrounded by Another Viscous Fluid", *Proceedings of the Royal Society of London. Series A, Mathematical and Physical* **150**(870) 322-337 (1935).
- Walker, J. and R. V. Calabrese. "The Effect of Surfactants On the Breakup of An Axisymmetric Laminar Jet" in "Interfacial Flows", Nashville. TN USA, 2009, AIChE Annual Meeting.

- Yang, H., C. C. Park, et al., "The coalescence of two equal-sized drops in a two-dimensional linear flow", *Physics of Fluids* **13**(5) 1087-1106 (2001).
- Yang, M. and R. V. Calabrese. "Simulation of Flow Field and Circulation Time Phenomena in a Batch Rotor-Stator Mixer " in "Novel Computational Methods in Mixing Research and Design", Nashville TN, USA, 2009, AIChE Annual Meeting.

Nomenclature:

- a_L , Langmuir constant
 C , concentration, mol/m³
CMC, critical micelle concentration, mol/m³
 D^* , dimensionless droplet diameter, $d_{\text{drop}}/d_{\text{jet},i}$
 D_{32}^* , dimensionless Sauter mean diameter, $D_{32}^* = \frac{1}{d_{\text{jet}}} \frac{\sum d_i^3}{\sum d_i^2}$
 d_{drop} , droplet equivalent spherical diameter, m
 d_i , diameter of droplet i , m
 $d_{\text{jet},i}$, initial jet diameter, m
 I_0 , modified Bessel function of the first kind, zeroth order
 I_1 , modified Bessel function of the first kind, first zero
 k , wavenumber, 1/m
 L_b , breakup length, m
 L_b^* , dimensionless breakup length, $L_b/d_{\text{jet},i}$
Oh, Ohnesorge number, $Oh = \frac{\mu}{\sqrt{\rho\sigma r_0}}$
 Q , volumetric flow rate, m³/s
 R , universal gas constant, 8.314472 J/(K·mol)
 r_0 , initial radius of jet, m
Re, Reynolds number, $Re = \frac{\rho U_n d_{\text{jet},i}}{\mu} = \frac{4\rho Q}{\pi d_{\text{jet},i} \mu}$
 T , Temperature, K
 U_n , initial jet velocity normal to the capillary opening, m/s
 w , dimensionless growth rate of capillary instabilities

Greek Symbols

- δ_0 , amplitude of initial perturbation responsible for jet breakup, m
 η , dimensionless wavenumber, $\eta = kr_0$
 η_{max} , most amplified dimensionless wavenumber
 Γ_∞ , equilibrium surface excess concentration, mol/m²
 μ , viscosity, cP
 ρ , density, kg/m³
 σ , interfacial tension, mN/m
 σ_{eq} , equilibrium interfacial tension, mN/m
 σ_0 , interfacial tension before exposure to surfactants, mN/m
 ω , growth rate of capillary instabilities, 1/s

List of Figures:

- Figure 1 - RANS simulation results for a Rotor-Stator Mixer
- Figure 2 - RANS simulation results for a Laminar Jet
- Figure 3 - Schematic diagram of jet with relevant geometry
- Figure 4 - Predicted Effect of Jet Velocity on Breakup Length
- Figure 5 - Surfactant geometry
- Figure 6 - Micelles
- Figure 7 - Determination of CMC and Γ_{∞} using Equation 7
- Figure 8 - Schematic Diagram of Experimental apparatus
- Figure 9 - Schematic Diagram of Pendant Drop apparatus
- Figure 10 - Dimensionless breakup length (L_b^*) vs. Reynolds number for a water in air jet
- Figure 11 - Effect of Reynolds number on Dimensionless Drop Size
- Figure 12 - Effect of Reynolds Number on Dimensionless Breakup Length for a 10 cSt Silicone oil jet into deionized water
- Figure 13 - Effect of Reynolds Number on Droplet Size Length for a 10 cSt Silicone oil jet into deionized water
- Figure 14 - RANS simulation results using the vof method
- Figure 15 - Effect of surfactant concentration on Jet Breakup Length - grouped by capillary diameter
- Figure 16 - Effect of surfactant concentration on Jet Breakup Length - grouped by flow rate
- Figure 17 - Effect of surfactant concentration on Droplet Size - grouped by capillary diameter
- Figure 18 - Effect of surfactant concentration on Droplet Size - grouped by flow rate
- Figure 19 - Effect of Surfactant Concentration on droplet diameter for a Rotor-Stator Mixer operating at low speed
- Figure 20 - Effect of Surfactant Concentration on Droplet Diameter for a Rotor Stator Mixer operating at high speed
- Figure 21 - Sample images from the three phase regimes

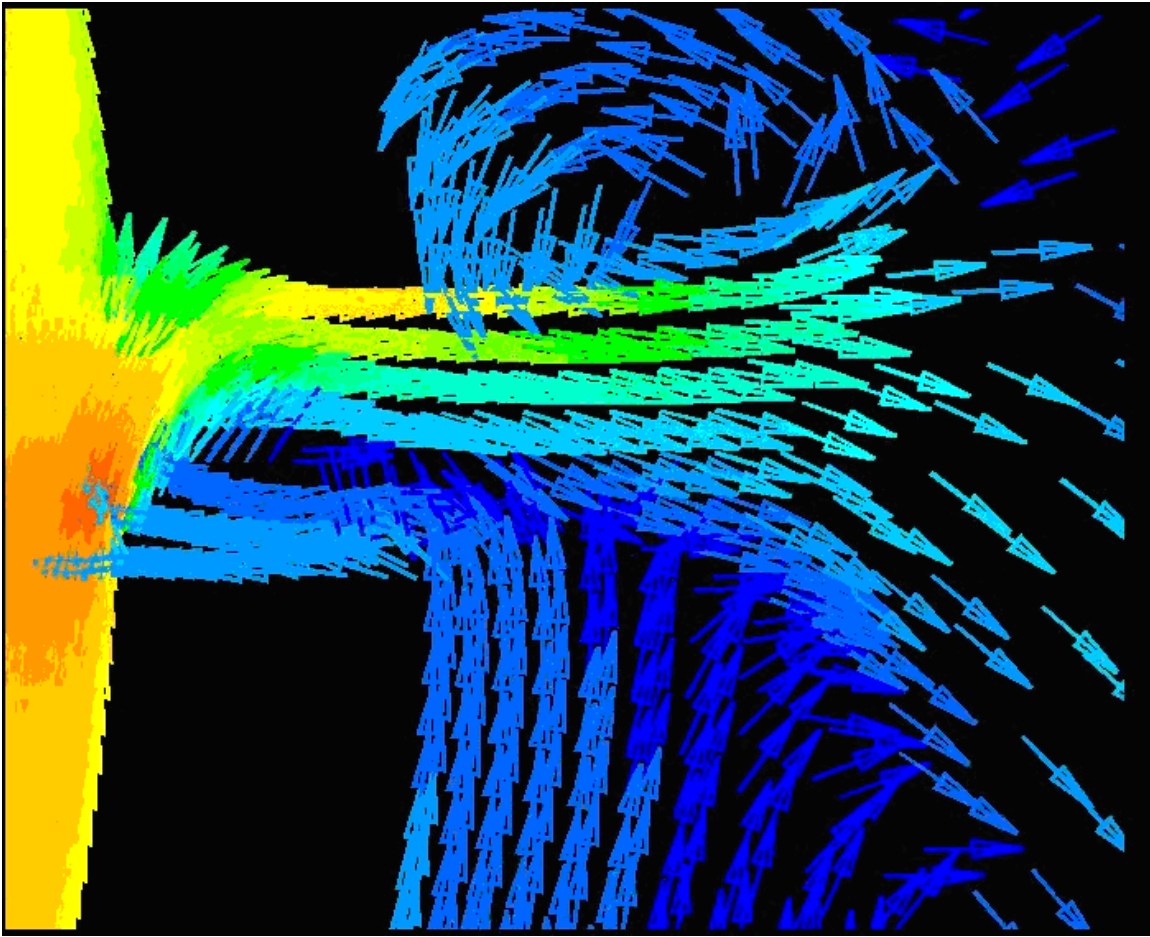


Figure 1 - RANS simulation results for a Rotor-Stator Mixer

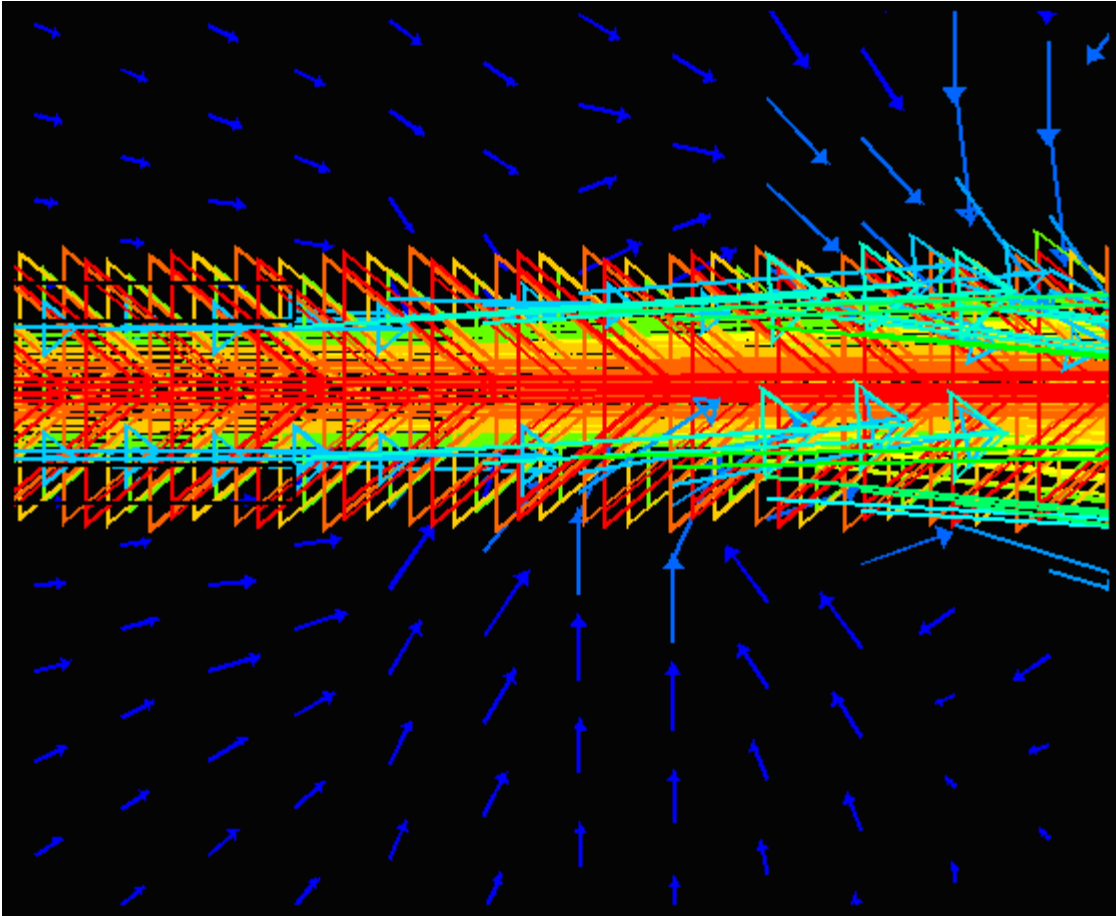


Figure 2 - RANS simulation results for a Laminar Jet

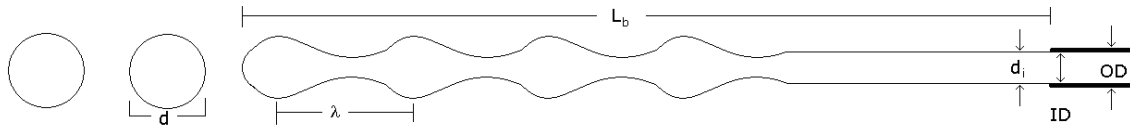


Figure 3 - Schematic diagram of jet with relevant geometry

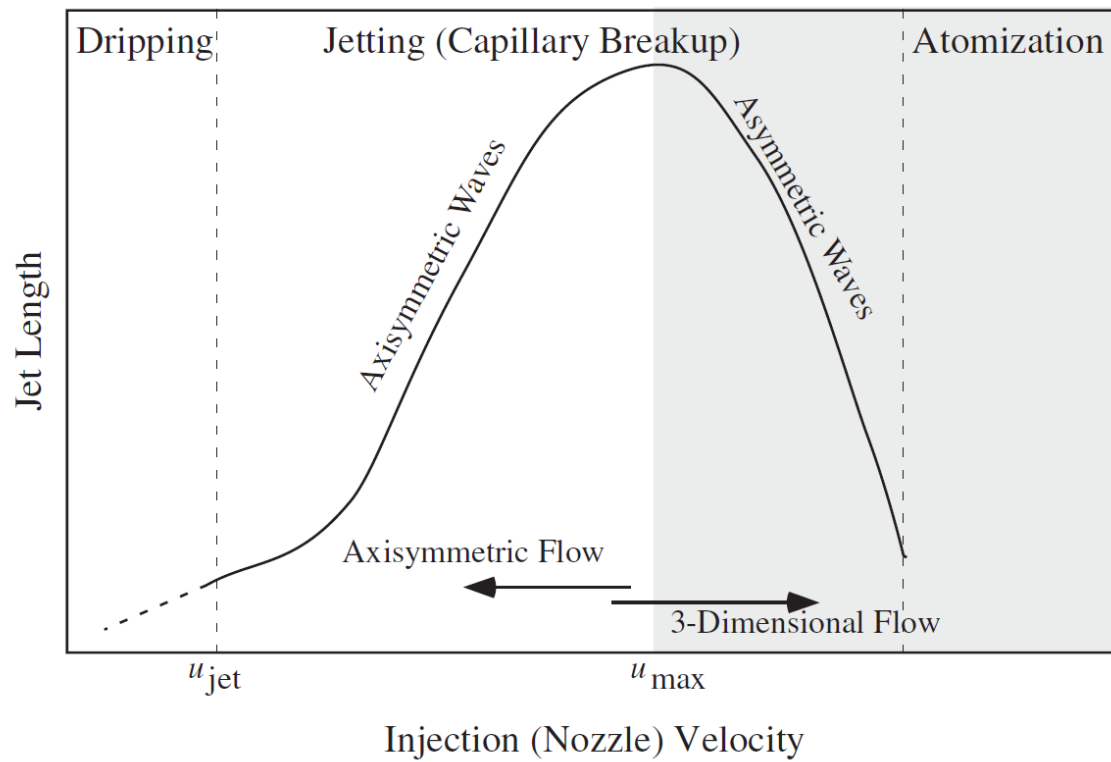


Figure 4 - Predicted Effect of Jet Velocity on Breakup Length

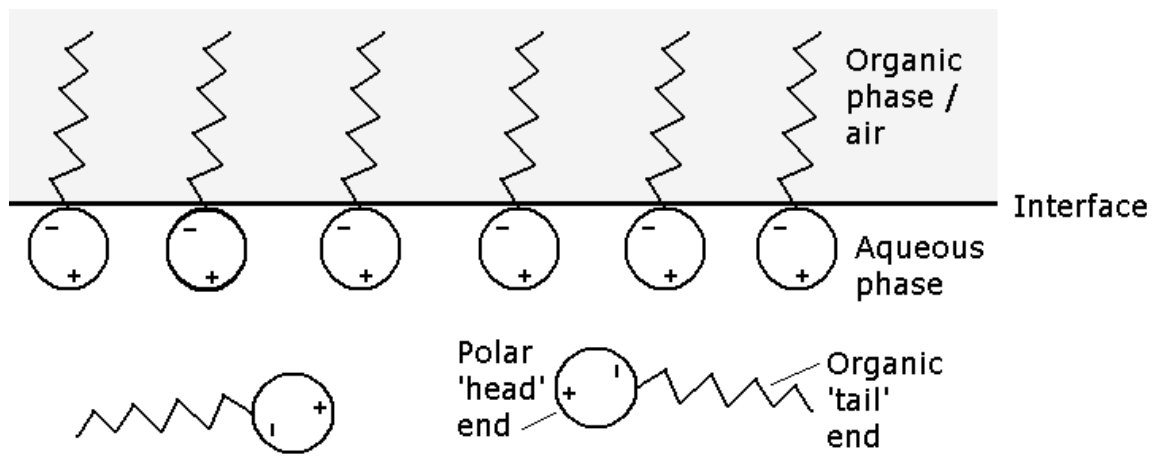


Figure 5 - Surfactant geometry

□ Aqueous Phase
■ Organic Phase

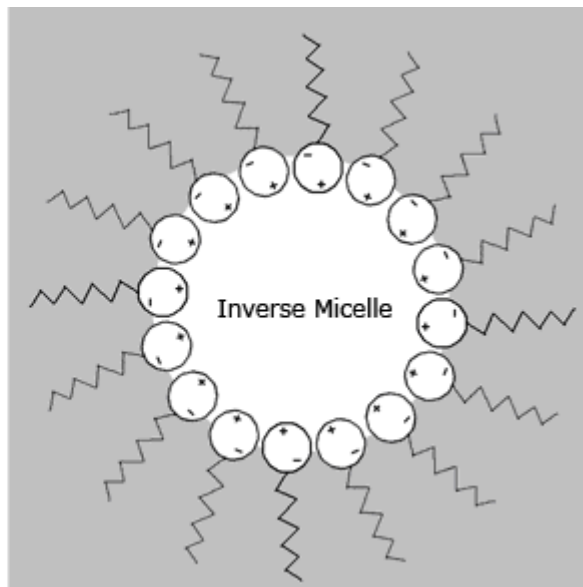
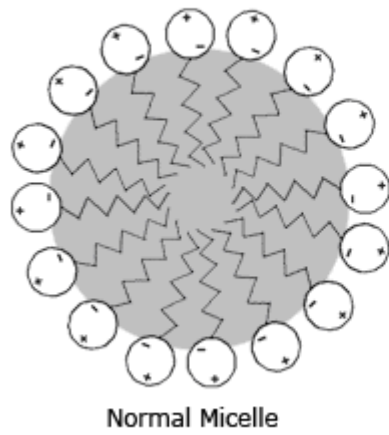


Figure 6 - Micelles

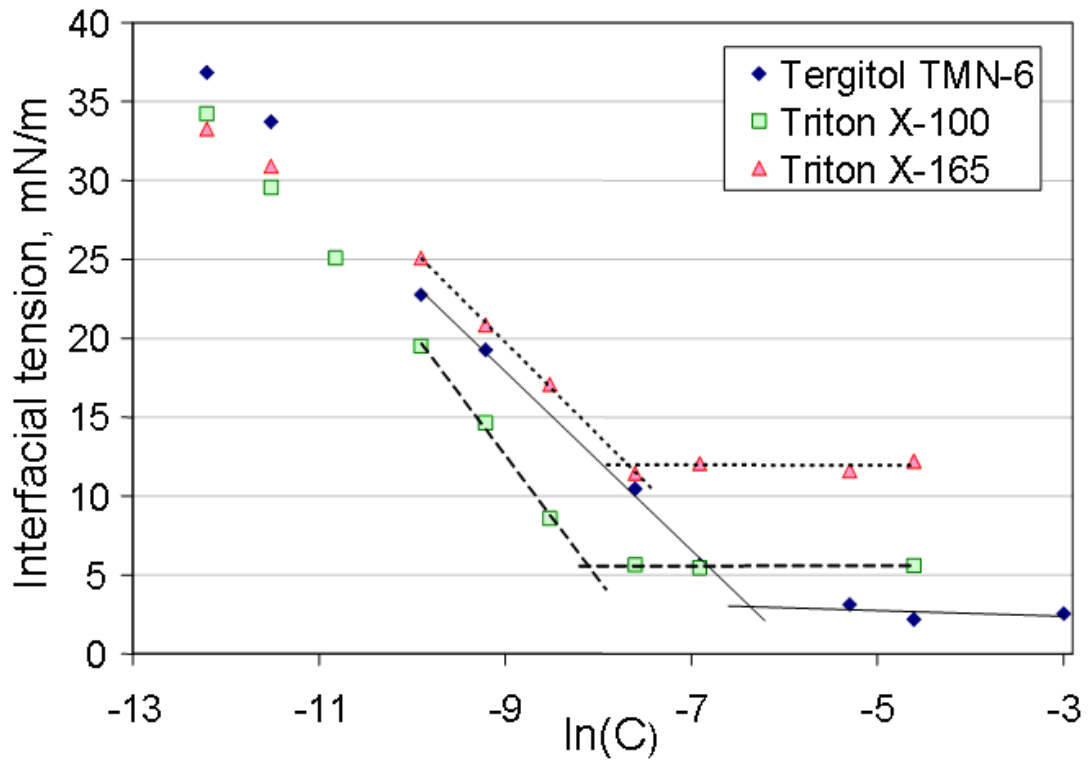


Figure 7 - Determination of CMC and Γ_{∞} using Equation 7

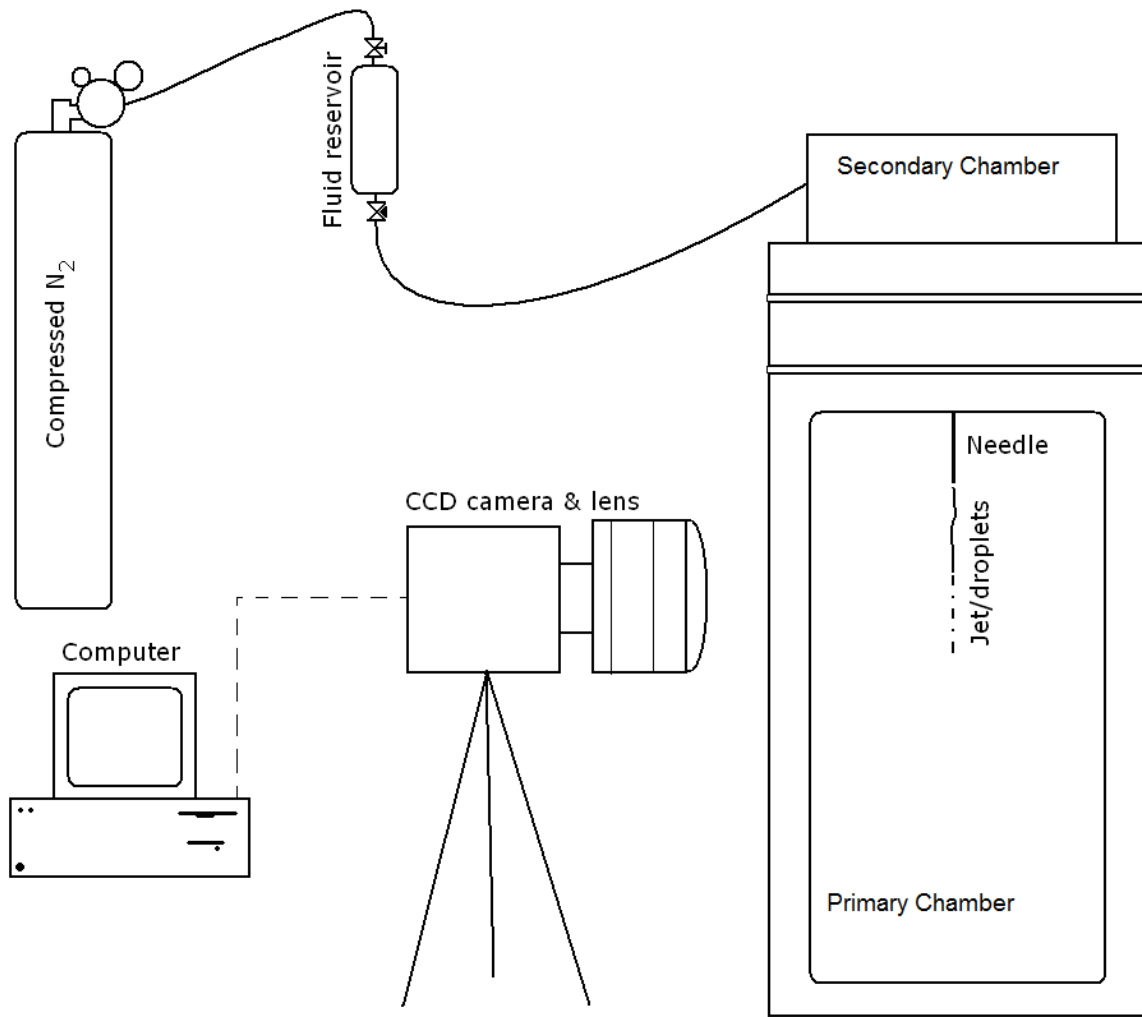


Figure 8 - Schematic Diagram of Experimental apparatus

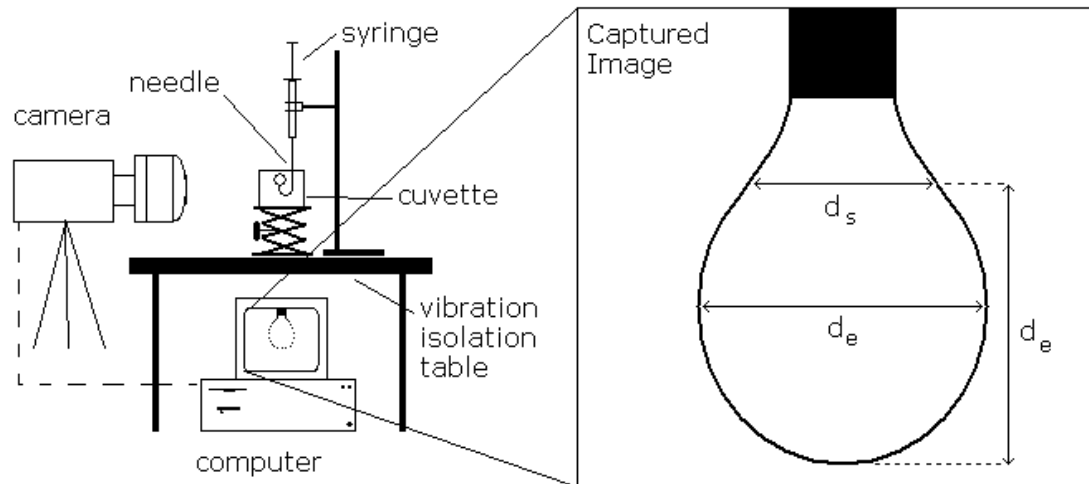


Figure 9 - Schematic Diagram of Pendant Drop apparatus

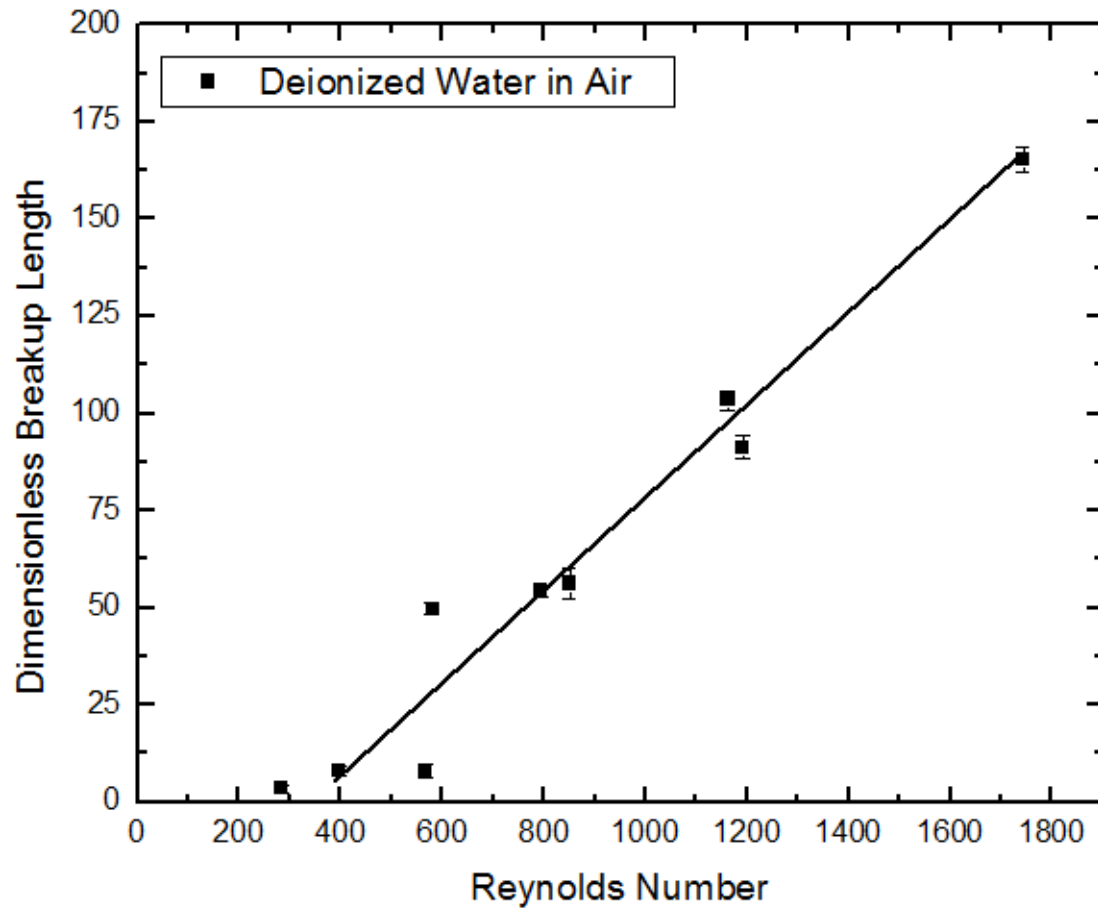


Figure 10 - Dimensionless breakup length (L_{b^*}) vs Reynolds number for a water in air jet

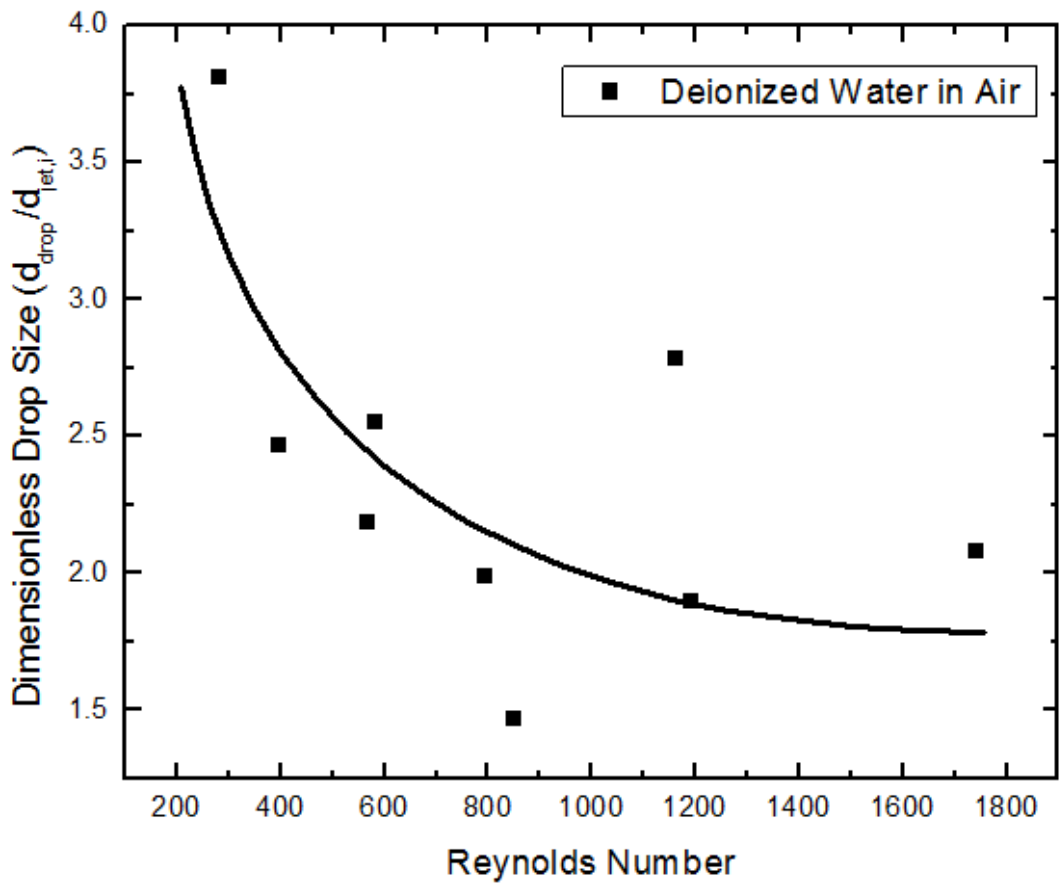


Figure 11 - Effect of Reynolds number on Dimensionless Drop Size

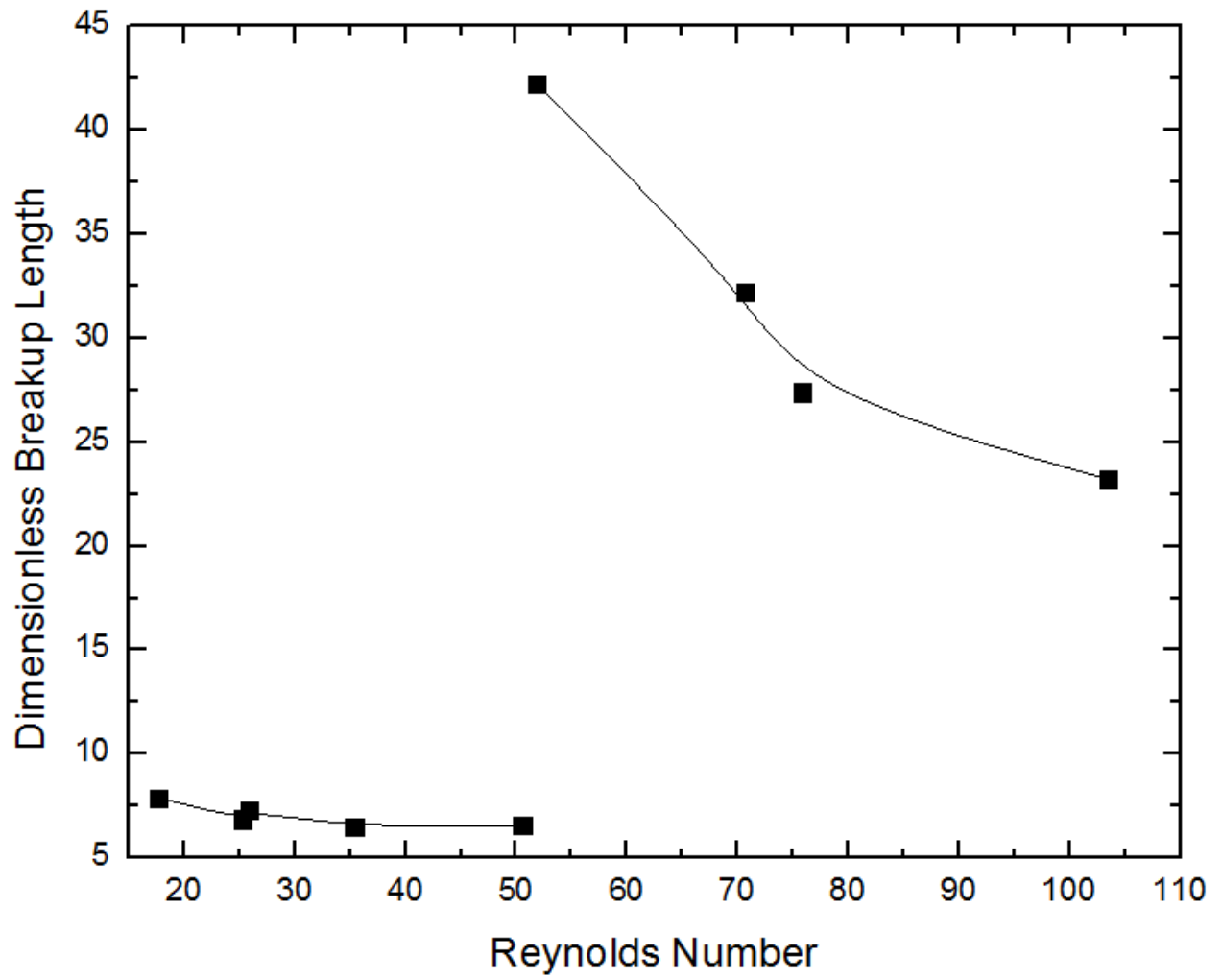


Figure 12 - Effect of Reynolds Number on Dimensionless Breakup Length for a 10 cSt Silicone oil jet into deionized water

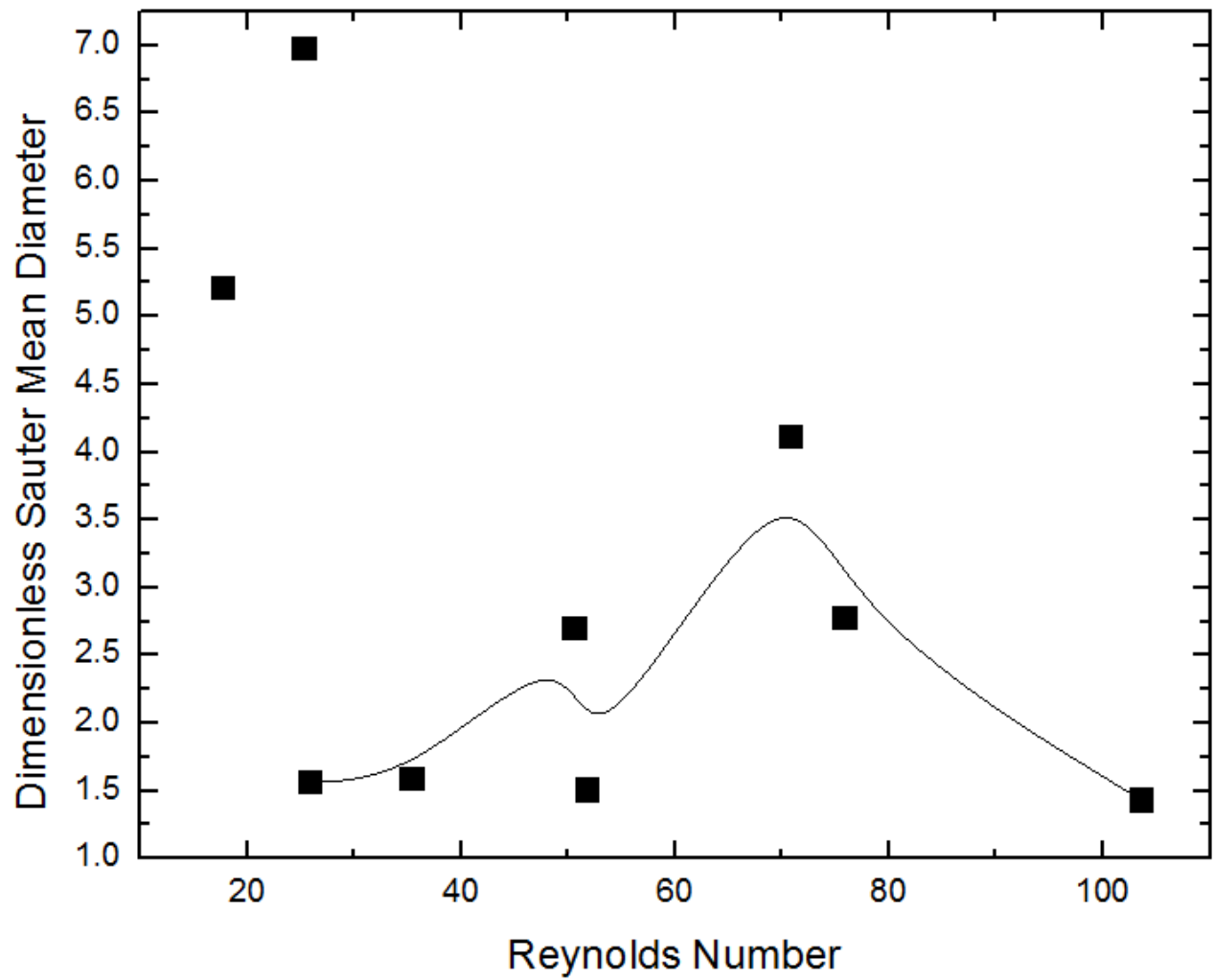
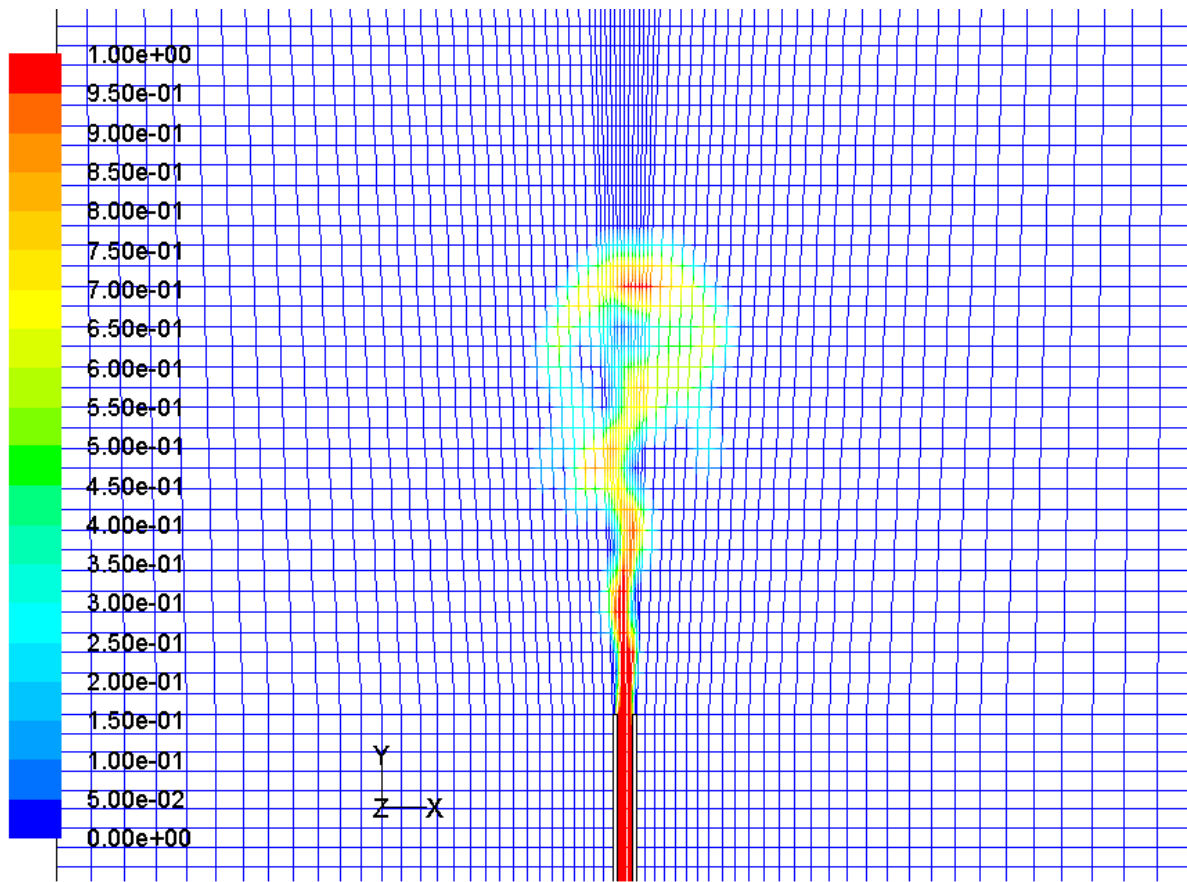


Figure 13 - Effect of Reynolds Number on Droplet Size Length for a 10 cSt Silicone oil jet into deionized water



Contours of Volume fraction (oil) (Time=1.8311e-01) Mar 15, 2010
ANSYS FLUENT 12.1 (2d, dp, pbns, vof, lam, transient)

Figure 14 - RANS simulation results using the vof method

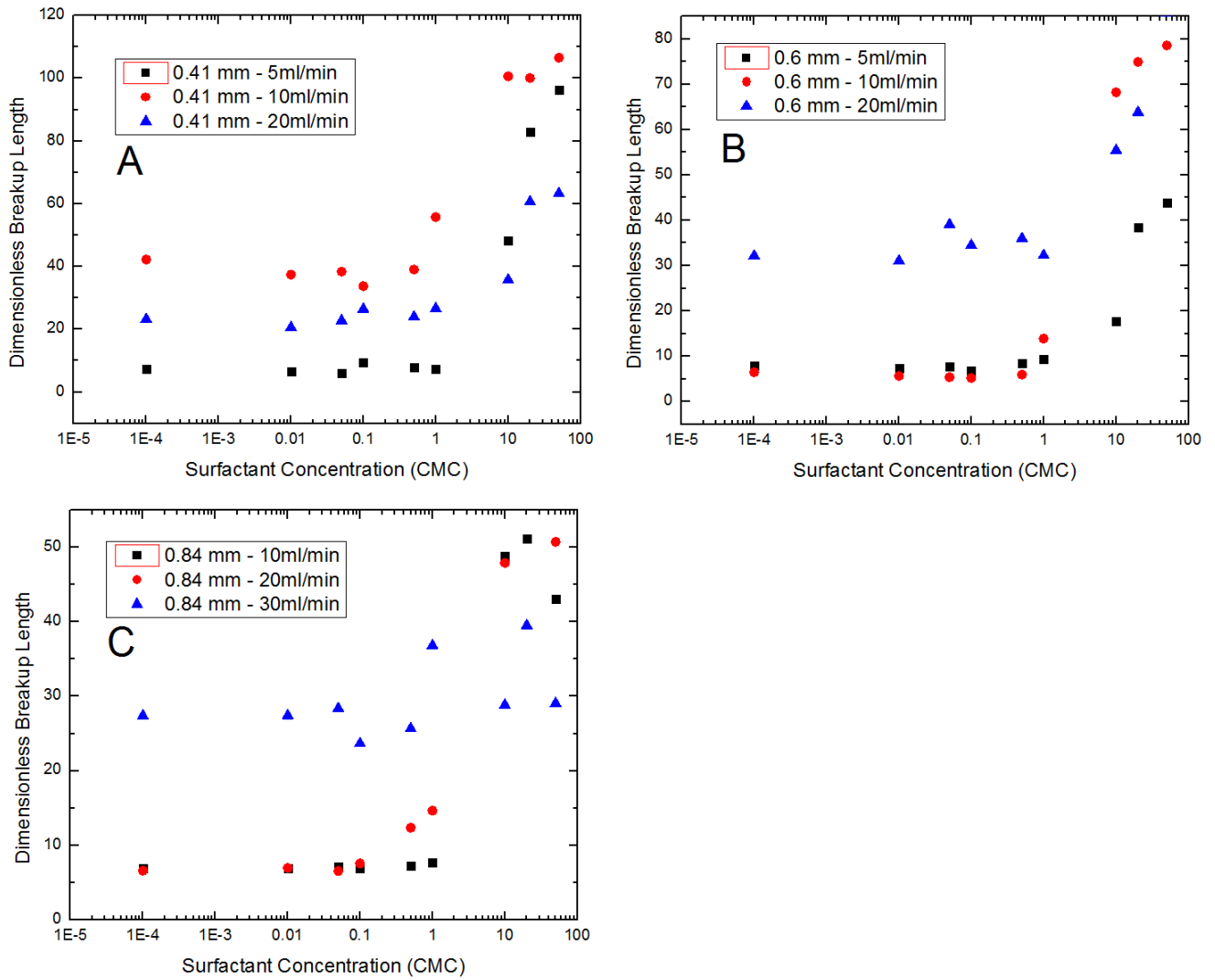


Figure 15 - Effect of surfactant concentration on Jet Breakup Length - grouped by capillary diameter

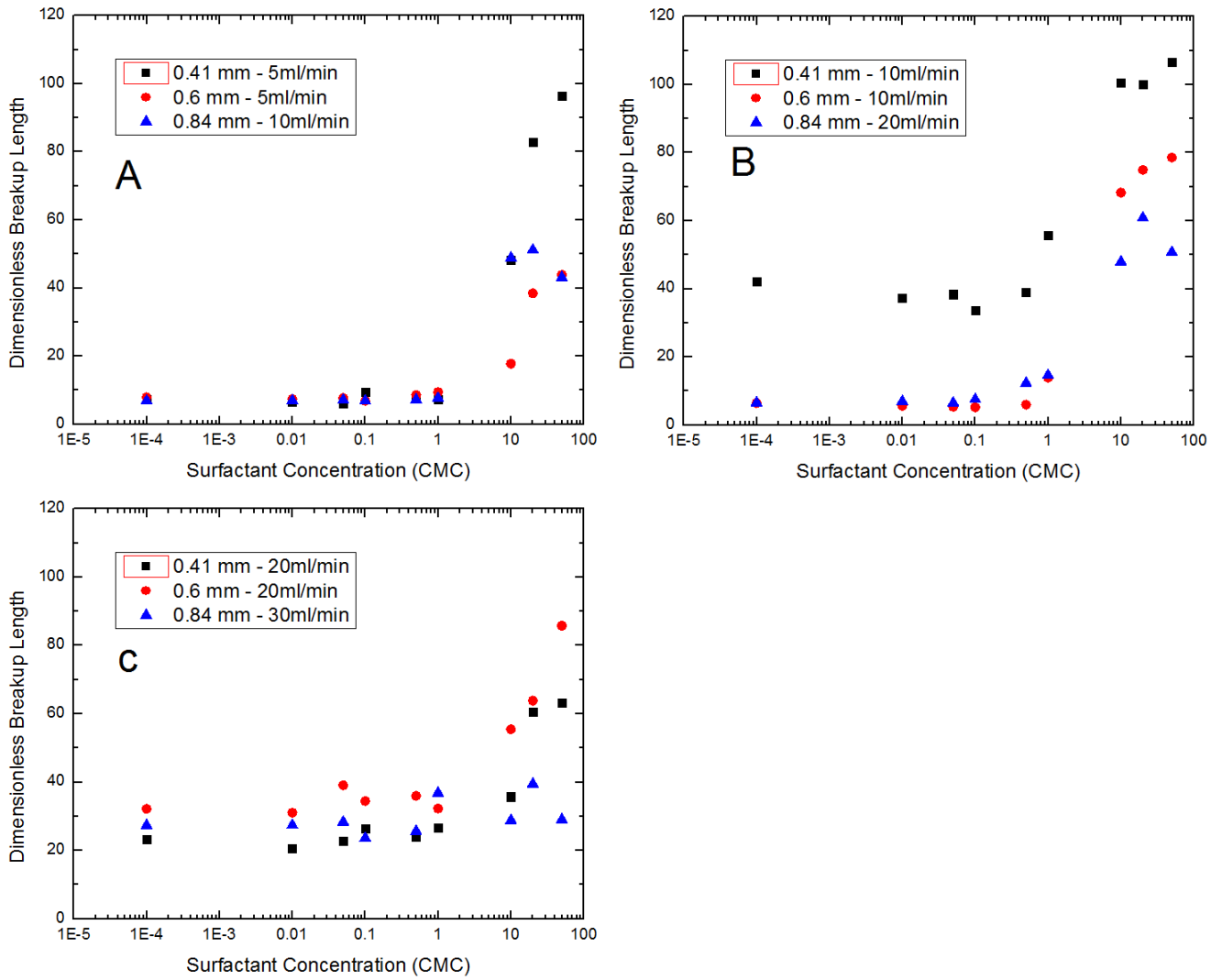


Figure 16 - Effect of surfactant concentration on Jet Breakup Length - grouped by flow rate

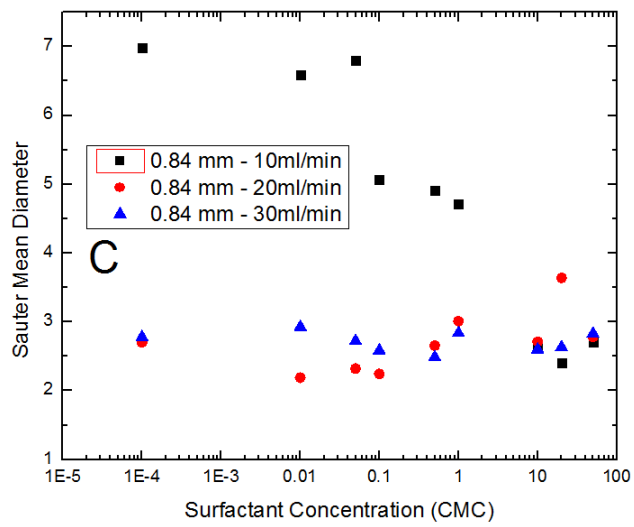
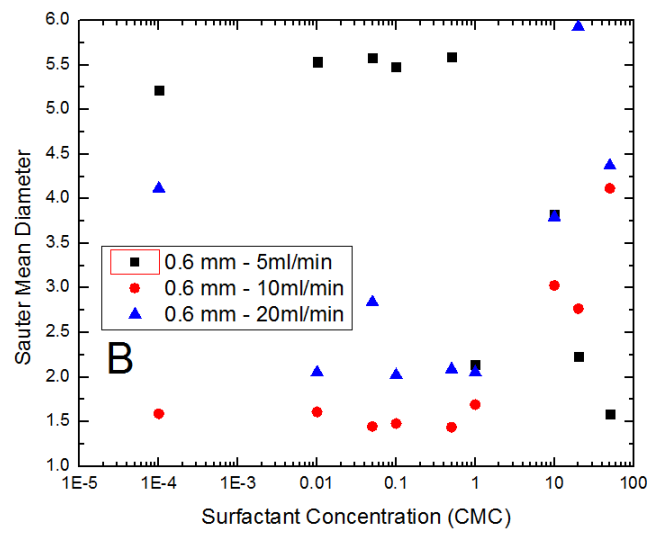
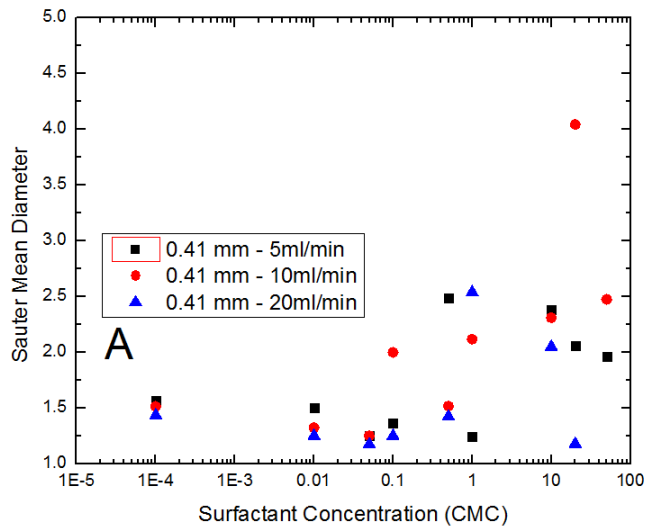


Figure 17 - Effect of surfactant concentration on droplet size - grouped by capillary diameter

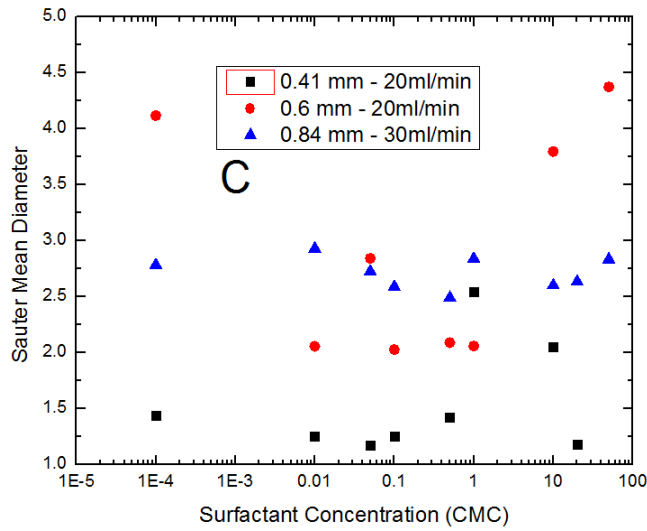
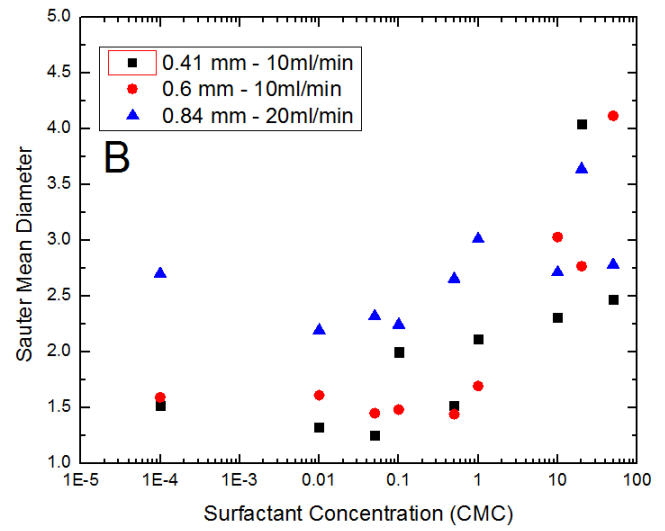
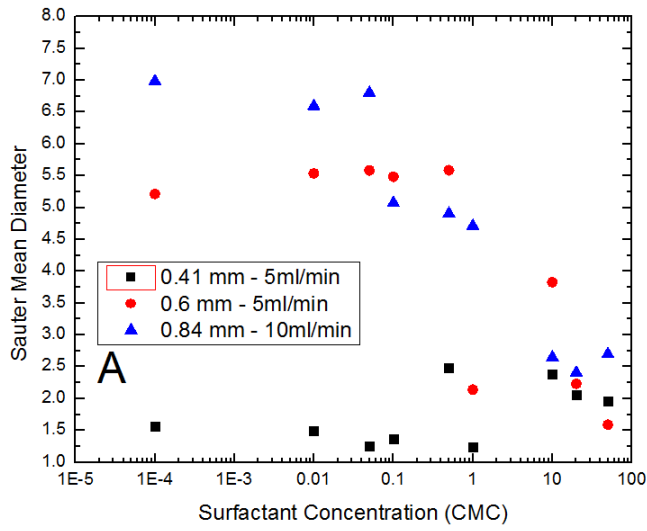


Figure 18 - Effect of surfactant concentration on droplet size - grouped by flow rate

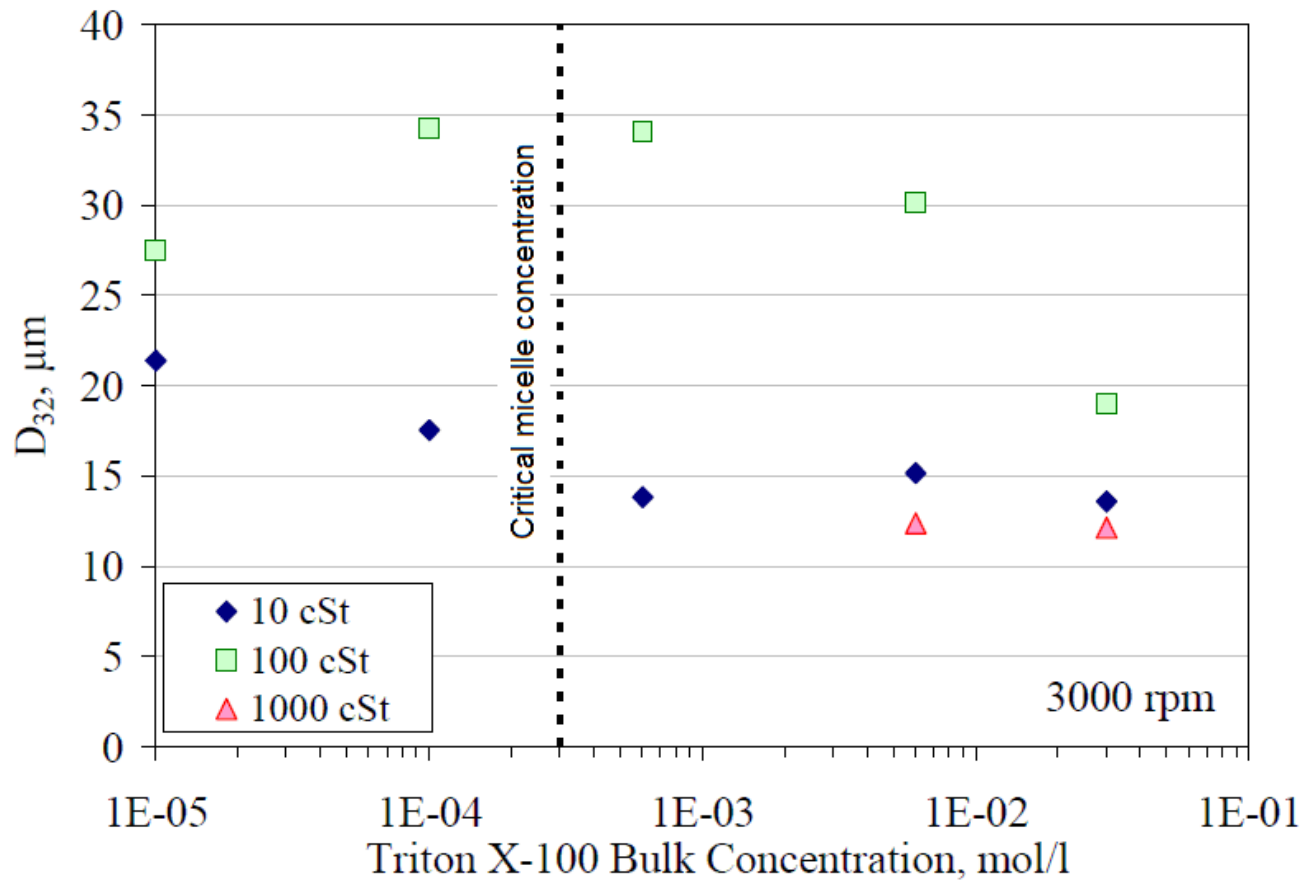


Figure 19 - Effect of Surfactant Concentration on droplet diameter for a Rotor-Stator Mixer operating at low speed

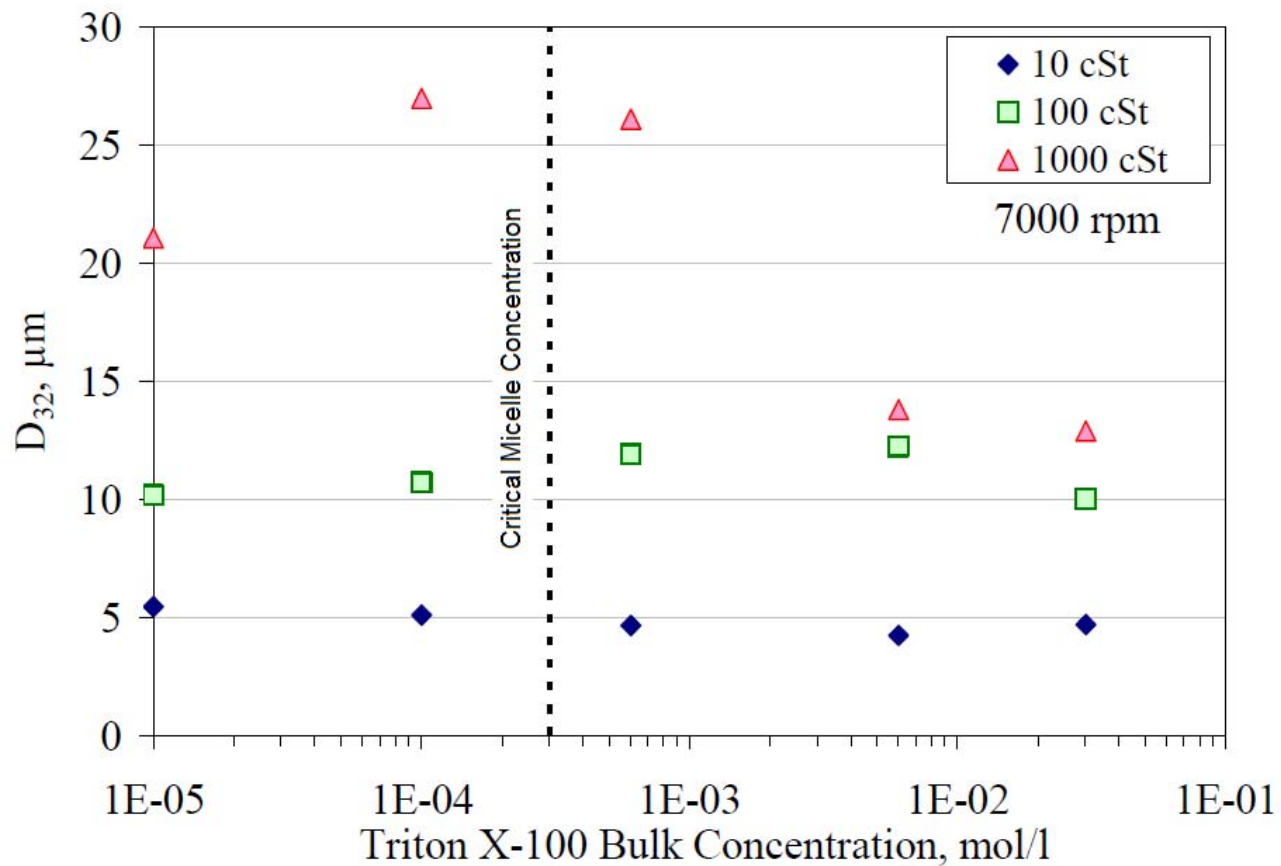


Figure 20 - Effect of Surfactant Concentration on Droplet Diameter for a Rotor Stator Mixer operating at high speed

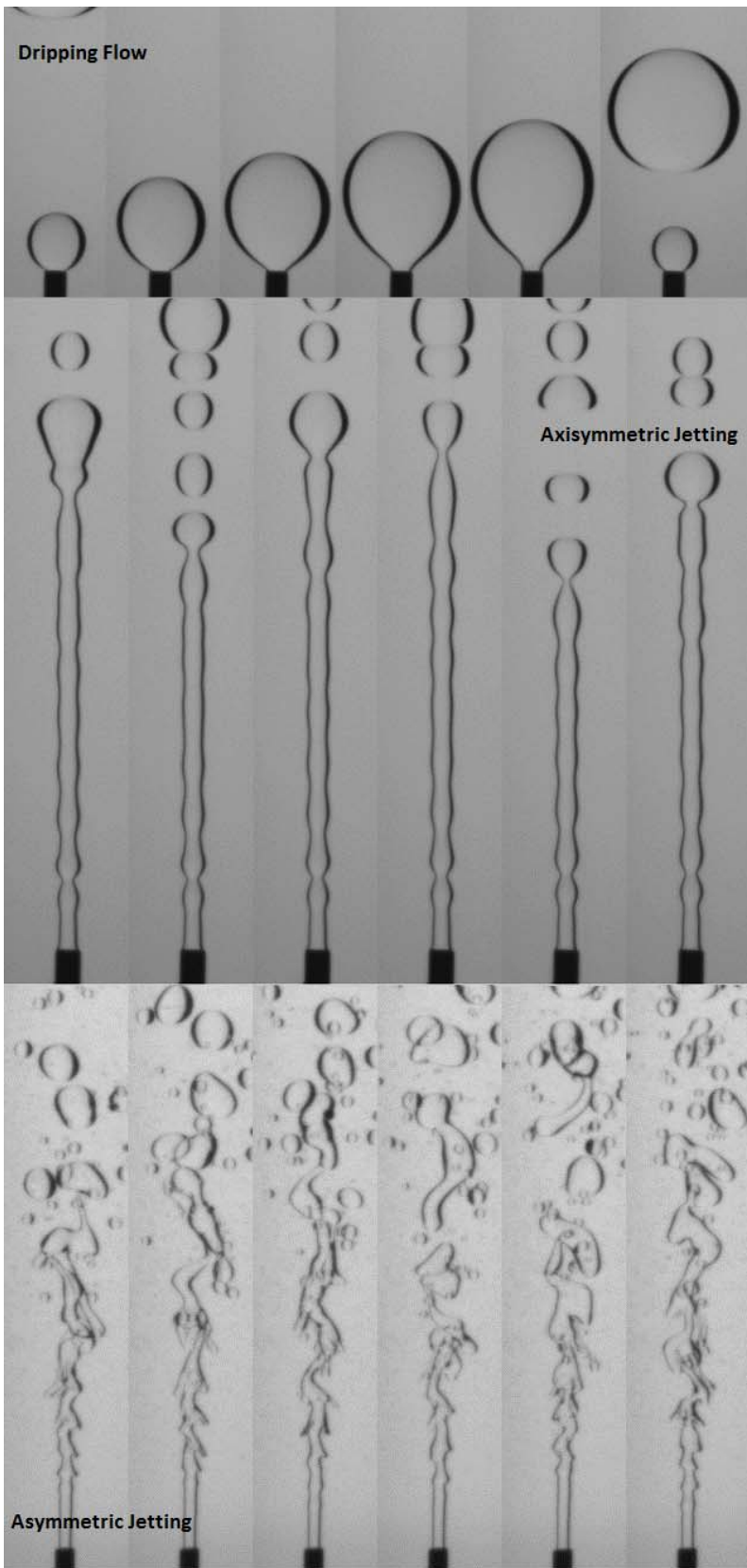


Figure 21 - Sample images from the three phase regimes